ChemPubSoc Europe

DOI: 10.1002/chem.201701783

CHEMISTRY A European Journal Communication

Water chemistry

Deactivation of a Cobalt Catalyst for Water Reduction through Valence Tautomerism

Habib Baydoun,[a] Shivnath Mazumder,[a, b] H. Bernhard Schlegel,[a] and Cláudio N. Verani*[a]

Abstract: The activity of the water reduction catalyst $[Co^{III}(L^1)(pyr)_2]PF_6$ (**1**), where $(L^1)^{2-}$ is a bis-amido pyridine ligand and pyr is pyrrolidine, is investigated. Catalyst **1** has an overpotential of 0.54 V and a high observed TOF of 23 min^{-1}, albeit for a relatively short time. Considering the significant activity of **1** and aiming to improve catalyst design, a detailed structural and electronic study is performed to understand the mechanisms of deactivation. Experimental and theoretical evidence support that the metal-reduced $[Co^{I}(L^1)]^-$ is in tautomeric equilibrium with the ligand-reduced $[Co^{II}(L^{1\bullet})]^-$ species. While $[Co^{I}(L^1)]^-$ favors formation of a $Co^{III}-H^-$ relevant for catalysis, the $[Co^{II}(L^{1\bullet})]^-$ species leads to ligand protonation, structural distortions, and, ultimatley, catalyst deactivation.

Substantial efforts have been directed towards the development of molecular catalysts for water reduction based on abundant and affordable 3d transition metals.[1] Such catalysts must withstand drastic electronic and structural changes from high to low redox states required for the hydride formation that precedes H_2 evolution. To this end, cobalt complexes have been extensively studied because of the energetically affordable stepwise conversions from $3d^6$ Co^{III} to $3d^8$ Co^{I} and back to $Co^{III}-H^-$ and $Co^{II}-H^-$ hydride species.[1b,c,g,j,k,2] As such, mechanistic understanding of catalytic pathways, including those of deactivation, becomes a necessary condition to the development of robust catalysts.

Our group has studied the mechanisms of several proton and water reduction cobalt catalysts, including some phenolate-rich Co^{III} $[N_2O_3]$ catalysts that served as the stepping stone to much improved pyridine-rich $Co^{II/III}$ $[N_2N^{py}_3]$ catalysts for water reduction that display a turnover number (TON) greater than 7000 mol^{-1}.[1c,3] We have gathered evidence that some molecular catalysts such as cobalt oximes[2d] are converted into nanoparticulates through ligand hydrolysis; triggered by radical-based mechanisms.[1b] Therefore, although the involvement of ligands in the catalytic cycle has been reported,[4] we conclude that radical formation may have deleterious effects on H_2 production.[5] Here we examine this issue in detail and suggest that formation of energetically equivalent valence tautomers, namely $[Co^{I}(L)]^- \leftrightarrow [Co^{II}(L^{\bullet})]^-$ offers additional conversion pathways that lead to catalyst deactivation.

In order to evaluate this hypothesis we examined the electronic and redox structure of the pseudo-octahedral $[Co^{III}L^1(pyr)_2]PF_6$ (**1**) complex, where $(L^1)^{2-}$ is the doubly deprotonated form of a bis-amido pyridine ligand and pyr denotes axially coordinated pyrrolidines, as shown in Scheme 1. Complex **1** was synthesized by adapting reported procedures,[6]

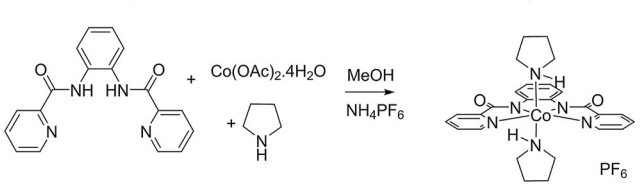

Scheme 1. Synthetic scheme of catalyst **1**.

where the ligand was treated under aerobic conditions with 1 equiv. of $Co(OAc)_2{\cdot}4H_2O$, in the presence of pyrrolidine, using methanol as the solvent. The formation of a microcrystalline precipitate was induced by the addition of NH_4PF_6. Complex **1** was thoroughly characterized using ^1H NMR, FTIR, ESI-MS(+), and elemental analysis (See Experimental Section for details), as well as X-ray crystallography (see below). As it will be discussed, this species is capable of robust water reduction followed by rapid deactivation.

The cyclic voltammogram (CV) of **1** was taken in CH_3CN and shows five independent redox processes (Figure 1). The processes at $E_{1/2} = 1.34\ V_{NHE}$ ($\Delta E = 0.10$ V, $|I_{pa}/I_{pc}| = 1.08$) and $E_{pa} = 1.94\ V_{NHE}$ are assigned as amido to amidyl radical oxidations[7] (for potentials vs. Ag/AgCl and Fc^+/Fc see Table S1 in Supporting Information).[8] The process at $E_{pc} = -0.32\ V_{NHE}$ is assigned to the Co^{III}/Co^{II} couple.[6b,9] The process at $-1.08\ V_{NHE}$ ($\Delta E_p = 0.16$ V, $|I_{pa}/I_{pc}| = 0.84$) is tentatively assigned to a Co^{II}/Co^{I} couple, while the third process at $-1.79\ V_{NHE}$ ($\Delta E = 0.11$ V) is attributed to a pyridine-based reduction.

The CV of **1** in phosphate buffer (1 mol L^{-1}, pH 7, Figure 2) shows a catalytic wave at $-0.95\ V_{NHE}$ in presence of **1** with concurent evolution of gas at the surface of the electrode. This

[a] H. Baydoun, Dr. S. Mazumder, Prof. H. B. Schlegel, Prof. C. N. Verani
Department of Chemistry, Wayne State University
5101 Cass Ave, Detroit, MI 48202 (USA)
E-mail: cnverani@chem.wayne.edu
Homepage: http://chem.wayne.edu/veranigroup/

[b] Dr. S. Mazumder
Current address:
Department of Chemistry, Hofstra University
Berliner Hall, Hempstead, NY 11549 (USA)

Supporting information and the ORCID identification number(s) for the author(s) of this article can be found under https://doi.org/10.1002/chem.201701783.

© 2017 Wiley-VCH Verlag GmbH & Co. KGaA, Weinheim

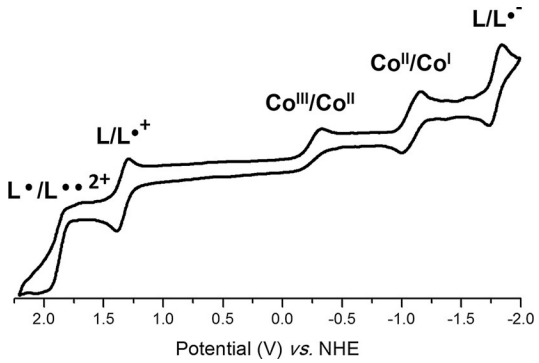

Figure 1. The CV of **1** (1 mM) in MeCN. Glassy carbon, Ag/AgCl, Pt wire, $TBAPF_6$ (0.1 M). Ferrocene is used as an internal standard.

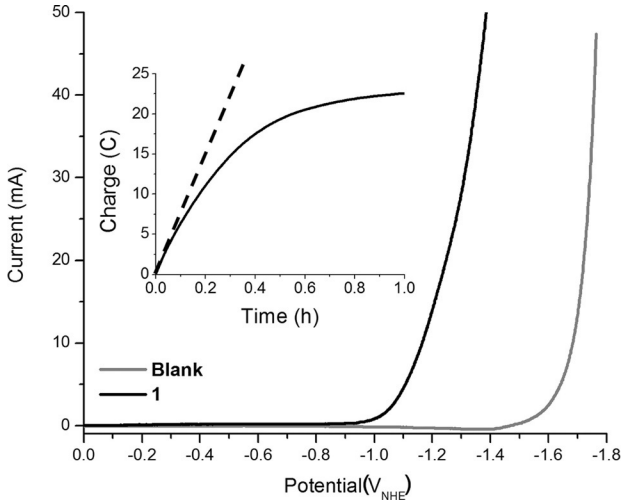

Figure 2. Polarization curve for **1** in phosphate buffer (1 mol L^{-1}, pH 7). Inset: Charge consumption over time for **1** (8 μmol L^{-1}) at −1.16 V_{NHE}. The dotted line represents an idealized charge consumption. Electrodes: Hg-pool (w), Pt (aux), Ag/AgCl.

corresponds to an overpotential of 0.54 V. Moreover, the onset potential of −0.95 V_{NHE} closely resembles that of the Co^{II}/Co^{I} couple observed at $E_{1/2} = -1.08$ V_{NHE} obtained in acetonitrile. This observation confirms that the active species in catalysis is the Co^{I} complex in accordance with the accepted mechanisms for proton reduction using cobalt metal complexes; catalysis is initiated by the reaction of Co^{I} with a proton to form a $Co^{III}-H^{-}$ hydride intermediate.[1b,c,g,j,k,2]

The identity of the evolved gas was determined as H_2 by means of gas chromatography following a bulk electrolysis experiment that was performed in an air-tight H-type cell (See Supporting Information for details).

The catalyst showed significant initial activity yielding a TON of 675 ± 30 after 30 min of electrolysis (turnover frequency, TOF = 23 min^{-1}) with a Faradaic efficiency of 97 ± 3%. However, this high activity persisted for only a short period of time. After ca. 30 minutes of catalysis, a considerable decrease in charge consumption was observed (Figure 2 inset). The observed TON is only a lower limit of the maximum value as it was measured following significant deacivation. Similar catalytic behavior has been observed for certain polypyridine frameworks.[10] Moreover, the solution changes color from green to colorless (Figure S1 a inset). Compared to the UV/Visible spectrum of the solution prior to catalysis, the post-catalytic spectrum shows the disappearance of charge transfer (CT) processes at ca. 413 nm associated with an $N_{amido} \rightarrow Co^{III}$ ligand-to-metal CT. However, the peaks associated with intraligand CT and observed below 300 nm persist (Figure S1). This suggests that the complex is undergoing demetallation. These observations prompted us to investigate the mechanism by which catalyst degradation takes place with the aim of providing guiding principles for future catalyst design.

Because the active form of the catalyst must contain Co^{I}, the elucidation of the deactivation pathways requires the investigation of the structural and electronic properties of the complex in distinct reduced oxidation states. To this end we used experimental observations along with DFT calculations. The structural information was obtained using potassium graphite (KC_8) as a stoichiometric reducing agent in order to isolate chemically the Co^{II} and Co^{I} reduced forms of our catalyst. Starting from **1** we were able to isolate the singly reduced Co^{II} analogue $[Co^{II}L^{1}(pyr)]^{o}$ (**2**) and the doubly reduced Co^{I} analogue $[Co^{I}L^{1}]K$ (**3**). We were able to grow X-ray quality crystals for **1**, **2**, and **3** (Figure 3). The structure of the Co^{III} species **1** (Figure 3 a) shows the expected pseudo-octahedral geometry, with the ligand $(L)^{-2}$ occupying the equatorial plane and the two pyrrolidines binding to the axial positions. Excellent agreement was observed between the obtained bond lengths and angles and that of structurally related complexes with a trivalent cobalt ion.[6a,b]

The structure of the Co^{II} species **2**, shown in Figure 3 b, on the other hand, displays a square pyramidal geometry in which $\tau = 0.018$.[11] This decrease from six- to five-dentate coordination upon reduction from Co^{III} to Co^{II} agrees with similar results from our group observed in oxime environments.[2d] Similarly, it is interesting to note that when compared to **1**, minor changes occur in the Co–L bond lengths, while a considerable 0.135 Å elongation takes place along the Co–N5 bond. The maintenance of the bond lengths within the equatorial plane suggests that upon metal-centered reduction from Co^{III} to Co^{II} the incoming electron is transferred to the unoccupied d_{z^2} orbital, while the electrons in the d_{xy}, d_{xz}, and d_{yz} orbitals remain largely unaffected, as previously proposed by our group.[2d] The $d_{x^2-y^2}$ orbital remains unoccupied. Moreover, the EPR spectrum of **2** (Figure 4 a) shows a signal with a *g* value of 2.018, which is consistent with the presence of one unpaired electron. Hence, the Co^{II} ion is found in a doublet $^{LS}3d^7$ configuration. This proposition was further examined by DFT calculations that showed excellent agreement between the crystal structure of **2** and the optimized structure of a doublet $^{LS}3d^7$ Co^{II} ion (Figure 4 b and c, and Figure S2 in Supporting Information).

The structure of **3** warrants some detailed discussion; unlike its 5-coordinate Co^{I} oxime congener,[2d] this doubly reduced derivative of **1** is composed of a tetracoordinate cobalt complex in a distorted square-planar geometry, where the maximal distortion between any two opposing planes among the Co–N bonds deviates by 9.5° from the idealized 0° (Figure 3 c).[12]

© 2017 Wiley-VCH Verlag GmbH & Co. KGaA, Weinheim

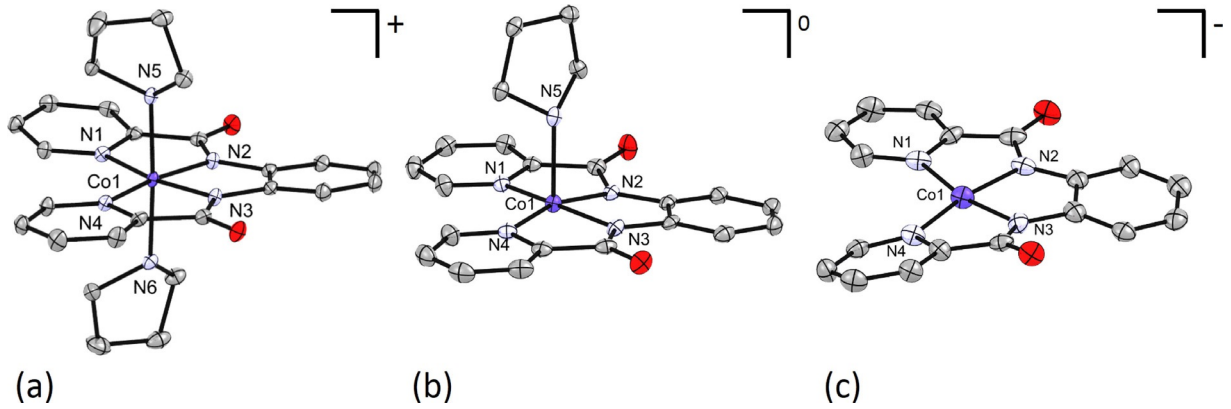

Figure 3. Crystal structures of **1** (a, CCDC 1533010), **2** (b, CCDC 1533009) and **3** (c, CCDC 1533008). Hydrogen atoms, solvents, and counter ions removed for clarity. Ellipsoids shown at 50% probability. Selected bond lengths for **1**: Co1–N1 1.9861(18), Co1–N4 1.9998(17), Co1–N2 1.8887(18), Co1–N3 1.8887(18), Co1–N5 2.0154(18), Co1–N6 2.0047(18) Å. For **2**: Co1–N1 1.971(2), Co1–N4 1.993(2), Co1–N2 1.882(2), Co1–N3 1.882(2), Co1–N5 2.139(2) Å. For **3**: Co1–N1 1.889(4), Co1–N4 1.892(4), Co1–N2 1.874(4), Co1–N3 1.865(4) Å.

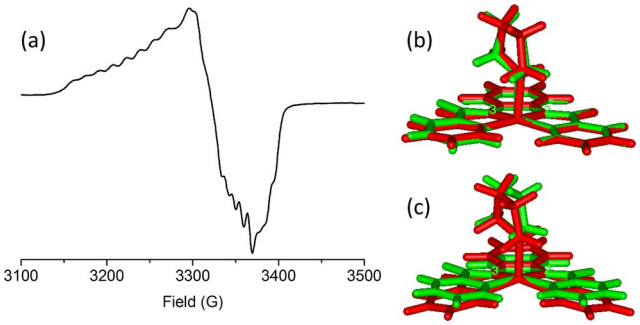

Figure 4. (a) EPR spectrum of **2** taken at 110 K in MeCN. Comparison of the crystal structure with the optimized structure of the calculated LS (b), and HS (c) structures.

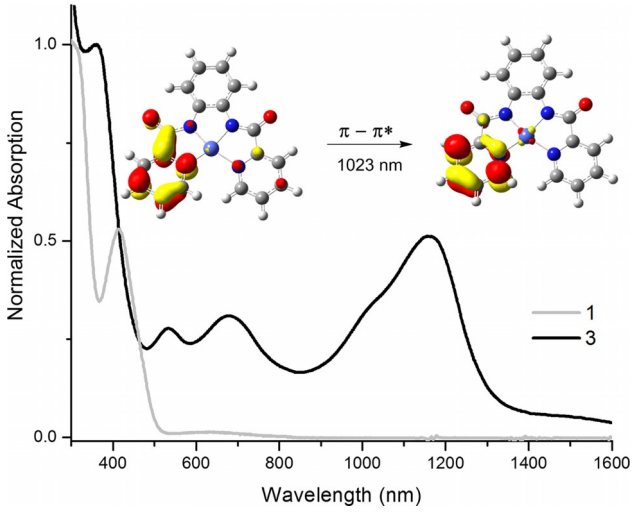

Figure 5. Normalized UV/Visible-NIR spectra of **1** (gray trace) and **3** (black trace) in MeCN. Inset: Calculated natural transition orbitals (NTOs at isovalue = 0.05 au) showing a π–π* intraligand CT transition at 1023 nm for **3** in acetonitrile solvent.

Compared to the previous two structures, the Co–N_{amide} bond lengths remain unchanged while its Co–$N_{pyridine}$ bond lengths are elongated by ca. 0.1 Å. Moreover, other bond lengths on the ligand framework remain largely unchanged (Figure S3). This observation implies that occupation of the d_{z^2} orbital is favored in the solid state, and that the structure contains a genuine $3d^8$ Co^I ion. Interestingly, DFT results indicate that two lowest lying isoenergetic states are possible for the nominal "Co^I species": 1) a metal-centered singlet species $[^{3d^8}Co^IL^1]^-$ akin to the crystal structure, or 2) a ligand-reduced and radical-containing triplet $[^{3d^7}Co^{II}(L^{1\bullet})]^-$ species with the unpaired electron centered on the amido-pyridine moiety. These two states display a calculated energy difference of ca. 3 kcal mol^{-1}, thus within the limits of the method (Figure S4). Furthermore, the $3d^8$ $[Co^IL^1]^-$ species yields a spin integers that is NMR active (Figure S5). However, comparison of the Co–N bond lengths, including those in the ligand framework, show better agreement with the metal-centered $[Co^IL^1]^-$ than with the ligand-reduced $[Co^{II}(L^{1\bullet})]^-$ species (Figures S6–S8).

Pivotal information necessary to probe the electronic nature of the reduced species comes from the UV/Visible-NIR spectra of **1**, **2**, and **3**. Figure 5 displays the spectra for **1** and **3**, while the spectrum of **2** is shown in Figure S9. As previously discussed, the spectrum of **1** shows a strong ligand to metal CT (LMCT) absorption at 413 nm. The spectrum of **2**, on the other hand, is characterized by an absorpion at 336 nm with a shoulder at 452 nm assigned to a $Co^{II}\rightarrow N_{amidopyridine}$ metal to ligand CT (MLCT) transition that confirms metal reduction. However, the spectrum of **3** also shows strong absorptions in the NIR region at 1028 and 1160 nm unquestionably attributed to ligand-stabilized radicals.[13] Complex **3** was independently generated through electrochemical reduction, and a spectrum with identical features was obtained (Figure S10) indicating that the same species can be conveniently obtained chemically or electrochemically. Therefore, analysis of these results suggest that in the solid state the $[Co^IL^1]K$ species prevails for **3**, while in an acetonitrile solution the species described as $[Co^{II}(L^{1\bullet})]K$ is accesible. This conclusion receives further support from time-dependent DFT calculations shown in Figures S11 and S12 of the Supporting Information where the simulated UV/Visible-NIR spectrum of $[Co^IL^1]^-$ lacks significant absorption processes above 800 nm, while the simulated spectrum for

© 2017 Wiley-VCH Verlag GmbH & Co. KGaA, Weinheim

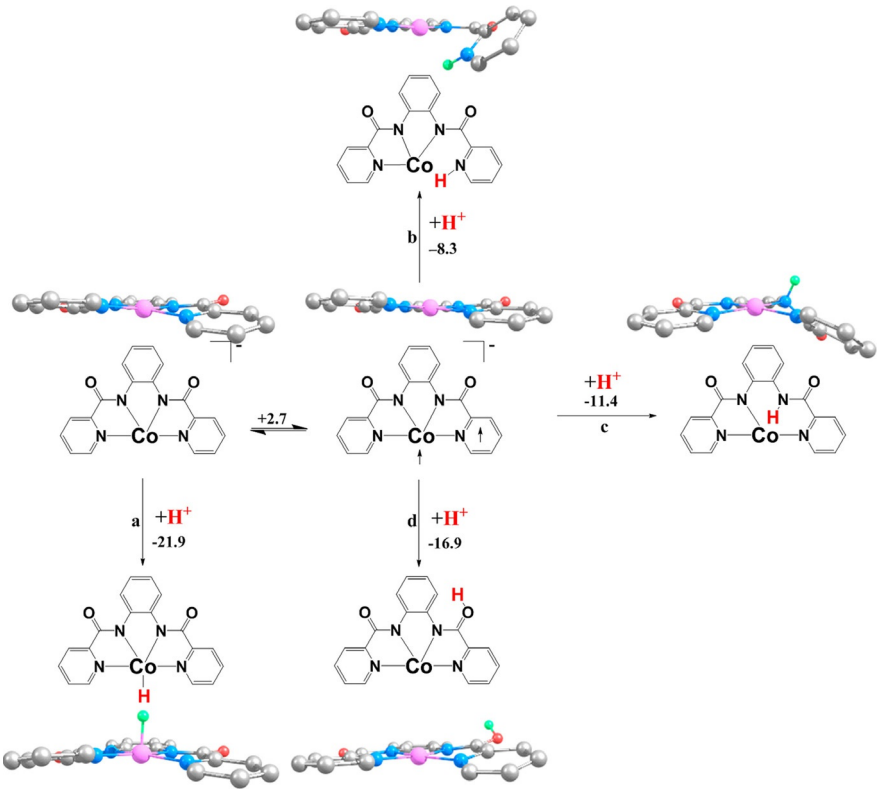

Figure 6. Energetics of protonation of the $[Co^{I}L^{1}]^{-}$ and $[Co^{II}(L^{1\bullet})]^{-}$ at different sites in water solvent. Free energies are reported in kcal mol^{-1}.

$[Co^{II}(L^{1\bullet})]^{-}$ shows absorption peaks at 1023 and 1205 nm of the NIR region. These transitions are mainly due to intraligand π–π^* charge transfers centered on the amidopyridine moiety shown in Figures 5 inset and Figure S13, respectively.

The small calculated energy difference of 2.7 kcal mol^{-1} between the two species is well within the limit of the DFT method, and coupled with the detection of $[Co^{I}L^{1}]K$ in the solid state and $[Co^{II}(L^{1\bullet})]K$ in acetonitrile, suggests that there is an equilibrium between the two states. Therefore, it is conceivable that both species will coexist under catalytic aqueous conditions. Such an equilibrium is consistent with the formation of valence tautomers.[14] As such, we propose that the difference in reactivity of the two tautomers with protons can be used to explain the deactivation of the catalyst. In presence of protons, the $[Co^{I}L^{1}]^{-}$ tautomer significantly favors the formation of a Co^{III}–H^{-} species (−22 kcal mol^{-1}), which is the first step in the catalytic cycle for H_2 production (Figure 6 pathway *a* and Figure S14). Conversely, concomitant formation of the $[Co^{II}(L^{1\bullet})]^{-}$ tautomer favors ligand protonation (Figure 6 pathways *b*–*d*). Upon such protonation of the ligand framework the structure deviates significantly from planarity (pathways *b* and *c*) with pathway *b* leading to a tridentate metal complex and from there to demetalation. These observations lead us to conclude that $[Co^{I}L^{1}]K$ is active in catalysis and leads to the formation of H_2, while $[Co^{II}(L^{1\bullet})]K$ is protonated, and eventually leads to the deactivation of the catalyst. This observation prompted us to hypothesize that running catalysis at a lower pH would favor protonation of the ligand and lead to deactivation. Indeed, catalytic runs at pH = 6 led to a faster decay in the consumption of charge over time associated with an overall decrease in activity (Figure S15–S16).

In summary, this work reports on a novel cobalt complex capable of performing water reduction at an overpotential of 0.54 V with TOF of 23 min^{-1} following 30 min of electrolysis with Faradaic efficiency of ca. 97 %. This initial catalytic activity decreases significantly after 30 minutes, and structural and electronic evaluation revealed that valence tautomerization is possible. The "Co^{I} state" can afford either $[Co^{I}L^{1}]^{-}$ or $[Co^{II}(L^{1\bullet})]^{-}$ within less than 3 kcal mol^{-1}. While the $[Co^{I}L^{1}]^{-}$ species supports the formation of a catalytically active Co^{III}–H^{-} species required for H_2 formation, the tautomer $[Co^{II}(L^{1\bullet})]^{-}$ favors ligand protonation accompanied by significant structural distortion that ultimately leads to catalyst deactivation associated with demetallation. These results allow us to postulate that efficient catalytic water reduction based on square planar ligands must proceed exclusively by means of the metal center while carefully avoiding ligand protonation. Current work in our labs builds on these results for the design of systems where the $[Co^{I}L^{1}]^{-}$ tautomer is energetically separated from its $[Co^{II}(L^{1\bullet})]^{-}$ tautomer.

Experimental Section

Synthesis of $[Co^{III}L^{1}(pyr)_2]PF_6$ (1)

A MeOH solution of $Co(OAc)_2{\cdot}4H_2O$ (1.6 g, 6.2 mmol) was added dropwise to a MeOH solution containing H_2L^{1} (2.0 g, 6.2 mmol, synthesis details in Supporting Information). To this mixture an excess

© 2017 Wiley-VCH Verlag GmbH & Co. KGaA, Weinheim

of 10 mL of pyrrolidine was added. The solution was allowed to stir overnight at room temperature. Then oxygen was bubbled into the solution for 5 minutes. The reaction mixture was filtered and an excess of NH_4PF_6 (1.5 g, 9.2 mmol) was added to precipitate **1**. X-ray quality crystals were grown through diethylether vapor diffusion into an acetonitrile solution of **1**. Yield: 86%; ^{1}H NMR (CD_3CN, 400 MHz): $\delta = 9.45$ (d, 2H), 8.90 (m, 2H), 8.41 (t, 2H), 8.29 (d, 2H), 8.00 (t, 2H), 7.12 (m, 2H), 3.22 (2H), 2.11 (4H), 1.53 (4H), 1.29 ppm (8H); IR (KBr): $\tilde{\nu} = 3167$ (ν_{N-H}), 1626 ($\nu_{C=O}$), 1599 and 1572 ($\nu_{C=N}$ and $\nu_{C=C}$), 844 cm^{-1} (ν_{PF_6}); ESI (m/z^+) = 517 for $[Co^{III}L^1(pyrrolidine)_2]^+$; elemental analysis calcd (%) for $C_{26}H_{30}CoN_6O_2PF_6$: C 47.14, H 4.56, N 12.69; found: C 47.05, H 4.44, N 12.49.

Synthesis of $[Co^{II}L^1(pyr)]^o$ (2)

$[Co^{II}L^1(pyr)]^o$ was isolated using standard glovebox techniques. A sample of **1** (108 mg, 0.16 mmol) was dissolved in THF and added into a vial containing KC_8 (22 mg; 0.16 mmol). The solution immediately changed from green to red and was allowed to stir for 2 h. The sample was filtered and a solution was obtained that yielded crude **2**. X-ray quality crystals were obtained by recrystallization in acetonitrile. Elemental analysis calcd (%) for $C_{22}H_{21}CoN_5O_2$: C 59.20, H 4.74, N 15.69; found: C 57.27, H 4.45, N 14.50.

Synthesis of $[Co^IL^1]K$ (3)

$[Co^IL^1]K$ was isolated in a similar way as for **2** using 44 mg of KC_8 (2 equiv; 0.32 mmol). The solution changed color from green to dark blue. X-ray quality crystals of **3** were obtained after filtration through slow evaporation from the THF solution. ^{1}H NMR (CD_3CN, 600 MHZ, Figure S5): $\delta = 9.36$ (2H), 8.37 (2H), 8.26 (t, 2H), 6.72 (2H), 6.53 (2H), 6.46 ppm (2H).

Water Reduction Experiments

Turnover numbers were determined using a custom built H-type bulk electrolysis setup. The cell consisted of two airtight compartments separated by a fine frit. One compartment was used to house the auxiliary electrode (Pt coil) while the other compartment was used to house the reference electrode (Ag/AgCl) and the working electrode (mercury pool). Before the application of a potential, the headspace was thoroughly purged with nitrogen gas. The amount of H_2 gas produced was determined by gas chromatography. In a typical experiment 100 μL of headspace was injected into the GC to determine the total amount of H_2. Turnover numbers were determined by dividing the total number of moles of hydrogen produced by the number of moles of catalyst used. The faradaic efficiency was determined by dividing the actual number of moles of hydrogen produced by the number of moles of hydrogen that should have been produced based on the charge consumed.

Computational Methods

Electronic structure calculations were carried out using the B3LYP* functional[15] as implemented in a development version of Gaussian.[16] The SDD basis set and effective core potential[17] were used for the Co atom and the 6-31G(d,p) basis set[18] was used for the other atoms. Solvation effects in acetonitrile and water were incorporated using the implicit SMD solvation model[19] and were included during structure optimization. All of the optimized structures were confirmed as minima by harmonic vibrational frequency calculations and the converged wave functions were tested for the SCF stability. The zero-point energy and thermal corrections were included for the calculation of the free energies. The standard states of 1 M concentration were considered for all the reactants and products for calculating the free energies of reactions. The literature value of -270.3 kcal mol^{-1} is used for the free energy of proton in water.[20] The spin density plots (isovalue = 0.004 au) were visualized using GaussView.[21] Vertical electronic excitation energies and intensities were evaluated using time-dependent DFT (TD-DFT)[22] and the orbital transitions of each excited state were characterized using the natural transition orbital (NTO) method.[23]

Acknowledgements

This material is based upon work supported by the U.S. Department of Energy, Office of Science, Office of Basic Energy Sciences under award number DE-SC0001907 to C.N.V. and H.B.S., including financial support for H.B. (synthesis, catalysis, and crystallography) and S.M. (calculations). The authors acknowledge Dr. Oleg Poluektov at Argonne National Labs for helpful EPR discussions. H.B. also acknowledges WSU-Chemistry for a Thomas C. Rumble Graduate Fellowship.

Conflict of interest

The authors declare no conflict of interest.

Keywords: amido-pyridine ligands · catalysis · cobalt complex · valence tautomerism · water reduction

[1] a) Y.-J. Yuan, J.-R. Tu, H.-W. Lu, Z.-T. Yu, X.-X. Fan, Z.-G. Zou, *Dalton Trans.* **2016**, *45*, 1359 – 1363; b) D. Basu, S. Mazumder, X. T. Shi, R. J. Staples, H. B. Schlegel, C. N. Verani, *Angew. Chem. Int. Ed.* **2015**, *54*, 7139 – 7143; *Angew. Chem.* **2015**, *127*, 7245 – 7249; c) D. Basu, S. Mazumder, X. Shi, H. Baydoun, J. Niklas, O. Poluektov, H. B. Schlegel, C. N. Verani, *Angew. Chem. Int. Ed.* **2015**, *54*, 2105 – 2110; *Angew. Chem.* **2015**, *127*, 2133 – 2138; d) P. Zhang, M. Wang, Y. Yang, D. Zheng, K. Han, L. Sun, *Chem. Commun.* **2014**, *50*, 14153 – 14156; e) P. Zhang, M. Wang, Y. Yang, T. Yao, L. Sun, *Angew. Chem. Int. Ed.* **2014**, *53*, 13803 – 13807; *Angew. Chem.* **2014**, *126*, 14023 – 14027; f) K. Kawano, K. Yamauchi, K. Sakai, *Chem. Commun.* **2014**, *50*, 9872 – 9875; g) Z. Han, R. Eisenberg, *Acc. Chem. Res.* **2014**, *47*, 2537 – 2544; h) A. Call, Z. Codolà, F. Acuña-Parés, J. Lloret-Fillol, *Chem. Eur. J.* **2014**, *20*, 6171 – 6183; i) P. Zhang, M. Wang, F. Gloaguen, L. Chen, F. Quentel, L. Sun, *Chem. Commun.* **2013**, *49*, 9455 – 9457; j) V. S. Thoi, Y. Sun, J. R. Long, C. J. Chang, *Chem. Soc. Rev.* **2013**, *42*, 2388 – 2400; k) M. Wang, L. Chen, L. Sun, *Energy Environ. Sci.* **2012**, *5*, 6763 – 6778; l) P. H. A. Kankanamalage, S. Mazumder, V. Tiwari, K. K. Kpogo, H. B. Schlegel, C. N. Verani, *Chem. Commun.* **2016**, *52*, 13357 – 13360; m) S. Mandal, S. Shikano, Y. Yamada, Y.-M. Lee, W. Nam, A. Llobet, S. Fukuzumi, *J. Am. Chem. Soc.* **2013**, *135*, 15294 – 15297.

[2] a) J. L. Dempsey, B. S. Brunschwig, J. R. Winkler, H. B. Gray, *Acc. Chem. Res.* **2009**, *42*, 1995 – 2004; b) J. L. Dempsey, J. R. Winkler, H. B. Gray, *J. Am. Chem. Soc.* **2010**, *132*, 16774 – 16776; c) J. L. Dempsey, J. R. Winkler, H. B. Gray, *J. Am. Chem. Soc.* **2010**, *132*, 1060 – 1065; d) D. Basu, S. Mazumder, J. Niklas, H. Baydoun, D. Wanniarachchi, X. Shi, R. J. Staples, O. Poluektov, H. B. Schlegel, C. N. Verani, *Chem. Sci.* **2016**, *7*, 3264 – 3278.

[3] D. Basu, M. M. Allard, F. R. Xavier, M. J. Heeg, H. B. Schlegel, C. N. Verani, *Dalton Trans.* **2015**, *44*, 3454 – 3466.

[4] a) A. Zarkadoulas, M. J. Field, C. Papatriantafyllopoulou, J. Fize, V. Artero, C. A. Mitsopoulou, *Inorg. Chem.* **2016**, *55*, 432 – 444; b) C. S. Letko, J. A. Panetier, M. Head-Gordon, T. D. Tilley, *J. Am. Chem. Soc.* **2014**, *136*, 9364 – 9376; c) L. M. A. Quintana, S. I. Johnson, S. L. Corona, W. Villatoro, W. A. Goddard, M. K. Takase, D. G. VanderVelde, J. R. Winkler, H. B. Gray, J. D. Blakemore, *Proc. Natl. Acad. Sci. USA* **2016**, *113*, 6409 – 6414.

© 2017 Wiley-VCH Verlag GmbH & Co. KGaA, Weinheim

[5] a) N. Kaeffer, A. Morozan, J. Fize, E. Martinez, L. Guetaz, V. Artero, *ACS Catal.* **2016**, *6*, 3727 – 3737; b) B. D. McCarthy, C. L. Donley, J. L. Dempsey, *Chem. Sci.* **2015**, *6*, 2827 – 2834; c) E. Anxolabéhère-Mallart, C. Costentin, M. Fournier, S. Nowak, M. Robert, J.-M. Savéant, *J. Am. Chem. Soc.* **2012**, *134*, 6104 – 6107.

[6] a) M. Amirnasr, K. J. Schenk, S. Meghdadi, *Inorg. Chim. Acta* **2002**, *338*, 19 – 26; b) S. Meghdadi, M. Amirnasr, M. H. Habibi, A. Amiri, V. Ghodsi, A. Rohani, R. W. Harrington, W. Clegg, *Polyhedron* **2008**, *27*, 2771 – 2778; c) D. J. Barnes, R. L. Chapman, R. S. Vagg, E. C. Watton, *J. Chem. Eng. Data* **1978**, *23*, 349 – 350.

[7] a) S. K. Dutta, U. Beckmann, E. Bill, T. Weyhermüller, K. Wieghardt, *Inorg. Chem.* **2000**, *39*, 3355 – 3364; b) U. Beckmann, E. Bill, T. Weyhermüller, K. Wieghardt, *Inorg. Chem.* **2003**, *42*, 1045 – 1056.

[8] R. R. Gagne, C. A. Koval, G. C. Lisensky, *Inorg. Chem.* **1980**, *19*, 2854 – 2855.

[9] R. Shakya, S. S. Hindo, L. Wu, M. M. Allard, M. J. Heeg, H. P. Hratchian, B. R. McGarvey, S. R. P. Da Rocha, C. N. Verani, *Inorg. Chem.* **2007**, *46*, 9808 – 9818.

[10] a) W. M. Singh, T. Baine, S. Kudo, S. Tian, X. A. N. Ma, H. Zhou, N. J. DeYonker, T. C. Pham, J. C. Bollinger, D. L. Baker, B. Yan, C. E. Webster, X. Zhao, *Angew. Chem. Int. Ed.* **2012**, *51*, 5941 – 5944; *Angew. Chem.* **2012**, *124*, 6043 – 6046; b) M. Vennampalli, G. Liang, L. Katta, C. E. Webster, X. Zhao, *Inorg. Chem.* **2014**, *53*, 10094 – 10100.

[11] A. W. Addison, T. N. Rao, J. Reedijk, J. van Rijn, G. C. Verschoor, *J. Chem. Soc. Dalton Trans.* **1984**, 1349 – 1356.

[12] An idealized square planar structure displays 0° between opposing angles, whereas an idealized tetrahedral structure displays those planes at 90°. See for example, S. Blanchard, F. Neese, E. Bothe, E. Bill, T. Weyhermüller, K. Wieghardt, *Inorg. Chem.* **2005**, *44*, 3636 – 3656.

[13] a) A. Kochem, H. Kanso, B. Baptiste, H. Arora, C. Philouze, O. Jarjayes, H. Vezin, D. Luneau, M. Orio, F. Thomas, *Inorg. Chem.* **2012**, *51*, 10557 – 10571; b) M. M. Allard, J. A. Sonk, M. J. Heeg, B. R. McGarvey, H. B. Schlegel, C. N. Verani, *Angew. Chem. Int. Ed.* **2012**, *51*, 3178 – 3182; *Angew. Chem.* **2012**, *124*, 3232 – 3236; c) C. C. Scarborough, S. Sproules, T. Weyhermüller, S. DeBeer, K. Wieghardt, *Inorg. Chem.* **2011**, *50*, 12446 – 12462; d) T. Storr, P. Verma, Y. Shimazaki, E. C. Wasinger, T. D. P. Stack, *Chem. Eur. J.* **2010**, *16*, 8980 – 8983; e) W. Kaim, *Coord. Chem. Rev.* **2011**, *255*, 2503 – 2513.

[14] a) D. A. Shultz in *Magnetism: Molecules to Materials II: Models and Experiments* (Eds.: J. S. Miller, M. Drillon), Wiley-VCH, **2003**, pp. 281 – 306; b) R. M. Buchanan, C. G. Pierpont, *J. Am. Chem. Soc.* **1980**, *102*, 4951 – 4957; c) R. D. Schmidt, D. A. Shultz, J. D. Martin, P. D. Boyle, *J. Am. Chem. Soc.* **2010**, *132*, 6261 – 6273.

[15] M. Reiher, O. Salomon, B. A. Hess, *Theor. Chem. Acc.* **2001**, *107*, 48 – 55.

[16] Gaussian Development Version, Revision H.35, M. J. Frisch, G. W. Trucks, H. B. Schlegel, G. E. Scuseria, M. A. Robb, J. R. Cheeseman, G. Scalmani, V. Barone, G. A. Petersson, H. Nakatsuji, X. Li, M. Caricato, A. Marenich, J. Bloino, B. G. Janesko, R. Gomperts, B. Mennucci, H. P. Hratchian, J. V. Ortiz, A. F. Izmaylov, J. L. Sonnenberg, D. Williams-Young, F. Ding, F. Lipparini, F. Egidi, J. Goings, B. Peng, A. Petrone, T. Henderson, D. Ranasinghe, V. G. Zakrzewski, J. Gao, N. Rega, G. Zheng, W. Liang, M. Hada, M. Ehara, K. Toyota, R. Fukuda, J. Hasegawa, M. Ishida, T. Nakajima, Y. Honda, O. Kitao, H. Nakai, T. Vreven, K. Throssell, J. A. Montgomery, Jr., J. E. Peralta, F. Ogliaro, M. Bearpark, J. J. Heyd, E. Brothers, K. N. Kudin, V. N. Staroverov, T. Keith, R. Kobayashi, J. Normand, K. Raghavachari, A. Rendell, J. C. Burant, S. S. Iyengar, J. Tomasi, M. Cossi, J. M. Millam, M. Klene, C. Adamo, R. Cammi, J. W. Ochterski, R. L. Martin, K. Morokuma, O. Farkas, J. B. Foresman, D. J. Fox, Gaussian, Inc., Wallingford CT, 2016.

[17] M. Dolg, U. Wedig, H. Stoll, H. Preuss, *J. Chem. Phys.* **1987**, *86*, 866 – 872.

[18] a) P. C. Hariharan, J. A. Pople, *Theor. Chim. Acta* **1973**, *28*, 213 – 222; b) M. M. Francl, W. J. Pietro, W. J. Hehre, J. S. Binkley, M. S. Gordon, D. J. DeFrees, J. A. Pople, *J. Chem. Phys.* **1982**, *77*, 3654 – 3665.

[19] A. V. Marenich, C. J. Cramer, D. G. Truhlar, *J. Phys. Chem. B* **2009**, *113*, 6378 – 6396.

[20] C. P. Kelly, C. J. Cramer, D. G. Truhlar, *J. Phys. Chem. B* **2006**, *110*, 16066 – 16081.

[21] R. Dennington, T. Keith, J. Millam, Semichem, Inc., Shawnee Mission, KS, **2009**.

[22] a) L. Petit, P. Maldivi, C. Adamo, *J. Chem. Theory Comput.* **2005**, *1*, 953 – 962; b) E. Runge, E. K. U. Gross, *Phys. Rev. Lett.* **1984**, *52*, 997 – 1000; c) R. E. Stratmann, G. E. Scuseria, M. J. Frisch, *J. Chem. Phys.* **1998**, *109*, 8218 – 8224.

[23] R. L. Martin, *J. Chem. Phys.* **2003**, *118*, 4775 – 4777.

Manuscript received: April 21, 2017
Accepted manuscript online: April 24, 2017
Version of record online: May 22, 2017

© 2017 Wiley-VCH Verlag GmbH & Co. KGaA, Weinheim